LA-UR-06-2355
Approved for public release;
distribution is unlimited.

March 27, 2006

Title: Comparison of Constitutive Models for PBX 9501

Author(s): Ralph Menikoff

Submitted to: To be determined

Comparison of Constitutive Models for PBX 9501

Ralph Menikoff

March 27, 2006

Abstract

A constitutive model for an explosive consists of three parts: equation of state of reactants, equation of state of products, and reaction rate. For the HMX based plastic-bonded explosive PBX 9501, three models have previously been calibrated and used in numerical simulations. Here, these three models are compared. General conclusions about models inferred from the comparison are presented.

1 Introduction

Constitutive models of an explosive are needed for reactive hydro simulations. Plastic-bonded explosives (PBX) are heterogeneous materials. For engineering calculations, the typical cell size is greater than the average grain size of the explosive. Consequently, coarse grain averages or homgenized models with effective burn rates are typically used. Due to the complicated detonation physics, models involve trade-offs related to the phenomena and applications they aim at describing. Most models are empirical and the trade-offs are based on heuristics. This leads to many different models for the same explosive.

Different researchers calibrate their favorite model to different experimental data. Furthermore, model parameters are often tweaked to obtain better agreement with a specific experiment. Adjusting parameters can compensate for model difficiencies. This improves the accuracy for interpolating between experiments and allows fine tuning the design of a particular application.

Without these problem specific adjustments, the predictive capability of the models is limited.

Comparing different models is the first step in assessing their relative strengths and weaknesses. Moreover, fitting forms of a model are often used to extrapolate beyond the range of available data. Differences between models give an indication of the sensitivity associated with fits to limited data.

Here we compare three models for high HMX (cyclo-tetramethylene-tetranitramine, $C_4H_8N_8O_8$, see [Gibbs and Popolato, 1980, pp. 42–51]) content plastic-bonded explosives. Two of the models are for PBX 9501, which consists by weight of 94.9% HMX + 2.5% nitroplasticizer + 2.5% estane + 0.1% stabilizer. The third model is for LX 14, which consists of 95% HMX + 5% estane. Differences in binder and HMX grain size distribution have slight affects on initiation sensitivity, mechanical properties and aging, but negligible effect on the equation of state and propagating detonation waves. In support of this perspective, we note that the measured reaction zone profiles are nearly the same for planar CJ (Chapman-Jouguet) detonation waves in the high HMX content explosives PBX 9501, PBX 9404 and EDC 37 [Gustavsen et al., 1998a].

The three constitutive models we consider are briefly described in section 2. The main results are presented in section 3. We first compare the equations of state (EOS) separately for reactants and products. Next the Hugoniot loci for the reactants and detonation loci of the products are shown. The von Neumann spike and CJ states are compared. Then the ZND (Zeldovich-von Neumann-Doering) wave profiles for a planar CJ detonation wave are compared. In addition, an aspect of the EOS models that affects some applications is the limited domain of the reactants in expansion. This is briefly discussed. In section 4 general conclusions inferred from comparing constitutive models are presented.

2 PBX 9501 models

The three models we consider all use a Mie-Grüneisen form for the equations of state,

$$P(V,e) = P_{\rm ref}(V) + \frac{\Gamma(V)}{V}\Big[e - e_{\rm ref}(V)\Big] \ ,$$

where the Grüneisen coefficient Γ is assumed to depend only on V. A thermodynamically consistent temperature then requires that the specific heat

at constant volume is a function of only entropy. The models differ in the fitting forms for the reference curves, P_{ref} and e_{ref}, Grüneisen coefficient and the specific heat.

All three models assume a single reaction progress variable, λ. Furthermore, pressure-temperature equilibrium is assumed for a partially burnt explosive, *i.e.*, $0 < \lambda < 1$. The reaction rate is taken to be a function of P, T and λ.

The domain of the partially burnt explosive equation of state is determined by the conditions that an equilibrium state exists and is unique. Uniqueness requires that the equations of state for the reactants and products are thermodynamically consistent. Non-existence typically arises due to the solid equation of state used for the reactants having a limited domain in expansion. This issue is discussed in a latter section.

A brief description of the models follows:

- Model I [Menikoff, 2006]
  Reactants EOS is based on Birch-Murnaghan form for the cold curve fit to HMX isothermal compression data [Menikoff and Sewell, 2004] with the initial density and sound speed adjusted to match PBX 9501. Analogous to the Debye model, C_V is taken to be a function of a scaled temperature $T/\theta(V)$, where $\Gamma(V) = -\mathsf{d}\ln(\theta)/\mathsf{d}\ln(V)$. At the initial density, the temperature dependence of C_V is fit to molecular dynamics calculations of Goddard et al. [1998, fig. 4.13]. A Sesame tablular EOS is used for the reactants. The table generated by Shaw [2004] is based on PBX 9501 overdriven detonation wave data [Fritz et al., 1996] and release wave data [Hixson et al., 2000] for high pressures ($P > 20\,\text{GPa}$) and cylinder and sandwich experiment data at lower pressures. The reaction model uses a first order Arrhenius rate of the form $(1-\lambda)\exp(-T_a/T)$. Parameters are based on the chemical HMX reaction rate [Henson et al., 2002].

- Model II [Lambert et al., 2006]
  The fitting forms developed by Davis [1998, 2000] are used for the reactants and products EOS. The reactants EOS is fit to Hugoniot data. The specific heat of the reactants is assumed linear in entropy. The products EOS is fit to overdriven detonation data and the Gurney energy for expansion. An empirical reaction rate is used of the form $(1-\lambda)^\nu P^n$ with a reaction order $\nu < 1$. Parameters are fit to Pop plot data (run-to-detonation distance as function of pressure) and rate stick

data for the curvature effect (detonation velocity as function of front curvature).

- Model III [Tarver et al., 1996]
  JWL (Jones-Wilkins-Lee) EOS are used for both reactants and products. Parameters for the reactants EOS are fit to low pressure ($P \lesssim 10\,\mathrm{GPa}$) Hugoniot data. The specific heat of the reactants is constant. Parameters for the products appear to be recalibrated from previous fit to cylinder data in order to fit overdriven detonation wave data. The ignition and growth burn model, based on heuristic of hot spots, is used for the reaction rate. It has a very fast ignition term and two growth terms of the form $\lambda^{\nu_1}(1-\lambda)^{\nu_2}P^n$. The reaction orders gives an effective volume averaged rate that accounts for unresolved surface area of a burn front. The rate parameters are calibrated to sideways plate push test for LX-14. The sideways plate push test is a variant on the cylinder and sandwich tests.

Reaction model I is based on a temperature dependent chemical rate. It gives a reaction zone profile for a planar CJ detonation wave consistent with experimental data [Menikoff, 2006]. The rate model is also compatible with shock desensitization experiments. However, shock temperature gives a bulk rate too low to describe a shock-to-detonation transition. The temperature dependent model could be used in meso-scale simulations of ignition in which hot spots due to the heterogeneites inherent in a PBX are resolved.

Models II and III have effective pressure dependent burn rates rather than temperature dependent chemical rate. They can reproduce ignition phenomena, such as Pop plot data. In addition model II is compatible with data on the curvature effect [Lambert et al., 2006]. However, simple pressure dependent burn models do not describe shock desensitization experiments. Effective burn models are meant to be used with coarse grids. They are not suitable for simulations in which hot spots are resolved.

Several remarks are in order:
1. The assumption of a single reaction progress variable is reasonable only for the short reaction time scale of prompt detonation phenomena. On the slower time scale of a cook-off experiment, a multi-step reaction mechanism is needed to fit the data.
2. Characterizing the reactants by an equation of state neglects the shear stress that a solid can support. This simplification is appropriate for high

pressure detonation phenomena. For weak (*i.e.*, low pressure) ignition stimuli, mechanical properties of the reactants are important.
3. Calibrating constitutive models involves highly non-linear fits to limited data with significant uncertainties. There is no natural metric that accounts for data on different thermodynamic variables from different types of experiments. Consequently, fits are subjective and fitting procedures are seldom fully described.
4. Empirical burn models are calibrated in conjunction with equations of state of the reactants and products. Using the reaction rate from one constitutive model with the equations of state from another, invariably leads to a less accurate model. This is a generic difficulty that arises when there is not a good theory for the underlying physics phenomena. The critical phenomena for heterogeneous explosives involves hot spots.
5. The JWL equation of state was developed around 1965 [Kury et al., 1965] to describe detonation products. The ease with which it can be calibrated to cylinder test data and its simplicity of form were advantageous at a time when the available computing power (speed and memory) was a fraction of the power of the ubiquitous PCs of today. Despite the many overly simple assumptions in the JWL EOS, it is still widely used.

3 Model properties

3.1 Reactants shock locus

The key experimental data used to calibrate the reactant EOS is the principal Hugoniot locus. Projections of the loci in the (u_p, u_s)–, (V, P)– and (P, T)–planes for the three models are shown in fig. 1. Experimentally, the shock velocity u_s and particle velocity u_p are measured; data points are shown in the figure. The jump conditions are used to obtain the specific volume V and the pressure P. There is a lot of low pressure data ($P < 10\,\mathrm{GPa}$) which can be fit in the (u_p, u_s)–plane by a straight line; see for example, [Gibbs and Popolato, 1980, p. 115, sec. 7.3]. Model III is compatible with the low pressure Hugoniot data.

The high pressure data shows that the Hugoniot locus is concave down in the (u_p, u_s)–plane. PBX 9501 is composed mostly of crystaline grains of HMX. The locus has the expected behavior for a molecular crystal. The calibrations for models I and II include the high pressure data. Despite the

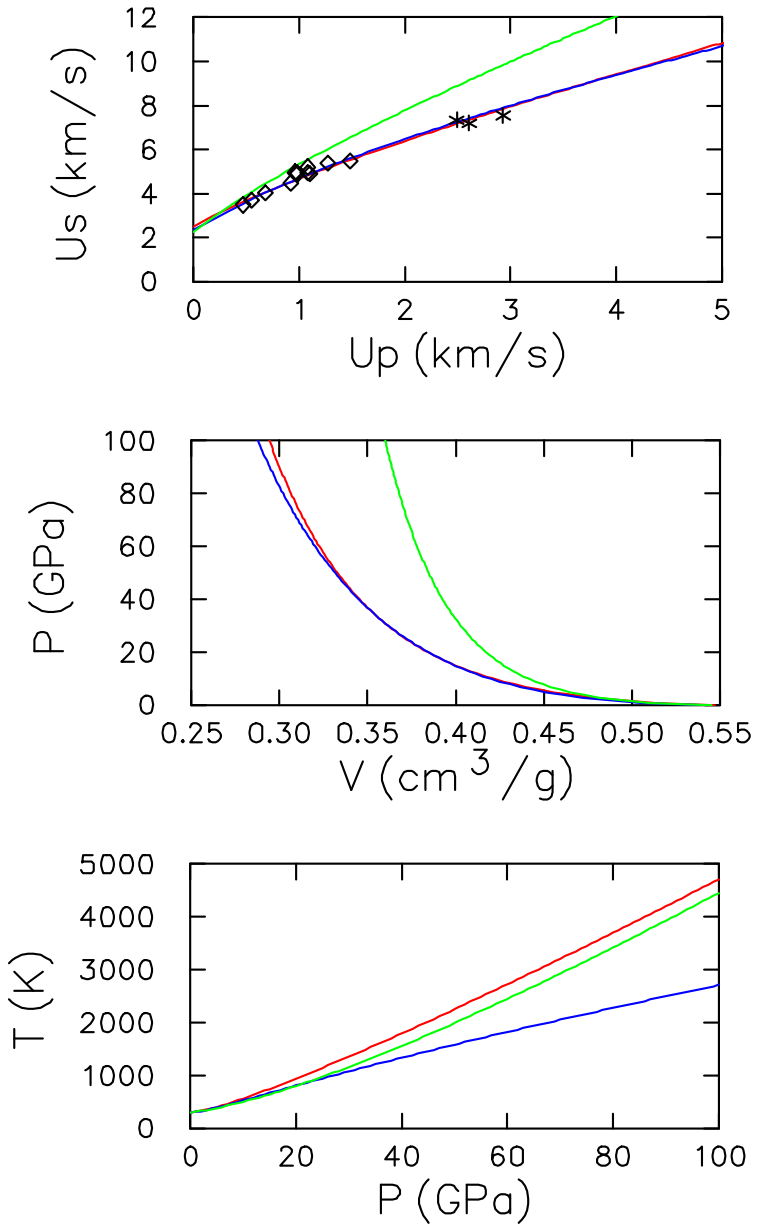

Figure 1: Reactant PBX 9501 Hugoniot loci: red, blue and green curves correspond to models I, II, III, respectively. Symbols in (Up, Us)–plane are experimental data points; diamonds are from Sheffield et al. [2004] and stars are from high pressure single crystal HMX experiments by Craig [Marsh, 1980, p. 595].

different fitting forms used, they are in good agreement. Model III is too stiff and not consistent with the data above 10 GPa. As discussed in a latter section, this has an important consequence for the reaction zone of a CJ detonation wave.

The shock temperature is inferred from the equation of state. The temperature as a function of pressure is similar for models I and III. This is fortutitous and the result of compensating errors; stiff EOS which lowers the specific energy and low specific heat which raises the temperature. To see this, we note that the temperature can be written as

$$T(V,e) = T_0 \exp\left[-\int_{V_0}^{V} \frac{\Gamma}{V}\,\mathsf{d}V\right] + \int_{e_s(V)}^{e} \frac{\mathsf{d}e}{C_v(V,e)}\ ,$$

where $e_s(V)$ is the energy on the initial isentrope; the first term arises from adiabatic compression and the second from shock heating. For strong shocks, $e \approx \frac{1}{2}u_p^2$, and at pressures below 100 GPa, e_s is approximately the area under the Hugoniot curve in the (V,P)–plane. Substituting the values of the parameters, one finds that the shock temperature is dominated by the specific heat term. Thus, for strong shocks, $T \propto \frac{1}{2}u_p^2/C_v$.

As is typical of EOS models for solids, model III assumes that the specific heat is constant. However, HMX is a large molecule and the specific heat is dominated by the intra-molecular vibrational modes. Consequently, the specific heat is temperature dependent. It varies by a factor of 2 between room temperature and the von Neumann spike temperature. Accounting for the temperature dependence of the specific heat is especially important when using a chemical reaction rate.

Physically, the specific heat should saturate at the classical limit; $C_V = 3\,N\,R$, where N is the number of atoms per molecule and R is the gas constant. Model II assumes that the specific heat is linear in entropy. For strong shocks, the model specific heat increases beyond the classical limit. Consequently, at high shock pressures, the specific heat is too high and the model temperature is too low.

Model I uses a Debye-like model for the vibrational modes. The model specific heat has the correct physical properties. However, there is no data available for shock temperature to compare with in order to assess the accuracy.

3.2 Products detonation and release loci

The data available to calibrate the products EOS consists of (i) release isentrope from the CJ state, (ii) overdriven detonation wave states, and (iii) release isentrope from an overdriven detonation wave. The overdriven detonation locus and the CJ isentrope for the three models are shown in fig. 2. Data points for overdriven detonation waves are also shown.

The CJ isentrope is measured indirectly. It is inferred from the transverse wall velocity behind an unsupported detonation wave in a cylinder test [Souers and Haselman, 1994] or sandwich test [Hill, 2002]. Hydro simulations are used to determine model parameters that give the best match to the measured time history for the wall velocity. Hence data points for the CJ isentrope are not shown on the figure.

The largest difference seen in fig. 2 is in plot of the sound speed. For model I, the decrease above 80 GPa is indicative of model defficiency due to limited domain of the fitting form used to construct the Sesame table. Wiggle near 20 GPa results from fitting different types of experiments; release wave from overdriven wave above pressure of 20 GPa and cylinder data below 20 GPa. The different experiments may have different systematic errors, or there may be non-equilibrium affects at the higher pressure.

Differences in the pressure appear small in the figure due to the large pressure scale. Since the adiabatic index (dimensionless sound speed, $\gamma = c^2/(PV)$) of explosive products at the CJ state is $\gamma \approx 3$, the differences among the models can be seen more clearly by plotting $P \times (V/V_0)^3$. The variations in the adiabatic index are also instructive. These are shown in fig. 3. For model I, $\gamma \approx 1$ at low density again indicates limited domain of fitting form used to construct the Sesame table. The differences in the pressure are significant with respect to the accuracy of the data. Comparison of the experimental data with simulated data is needed to assess the accuracy of each model. Such simulations are beyond the scope of this paper.

Many JWL EOS fits are available for explosive products. It is instructive to compare two fits for LX 14; parameters from model III [Tarver et al., 1996, table 2] and from [Souers and Haselman, 1994, table 5-3]. Key variables are shown in fig. 4. The parameters from [Souers and Haselman, 1994] have been optimized for pressures below the CJ state by calibrating to cylinder data. For model III the parameters have been modified to account for high pressure overdriven detonation wave data.

Two general points are noteworthy. First, the fitting form provides a

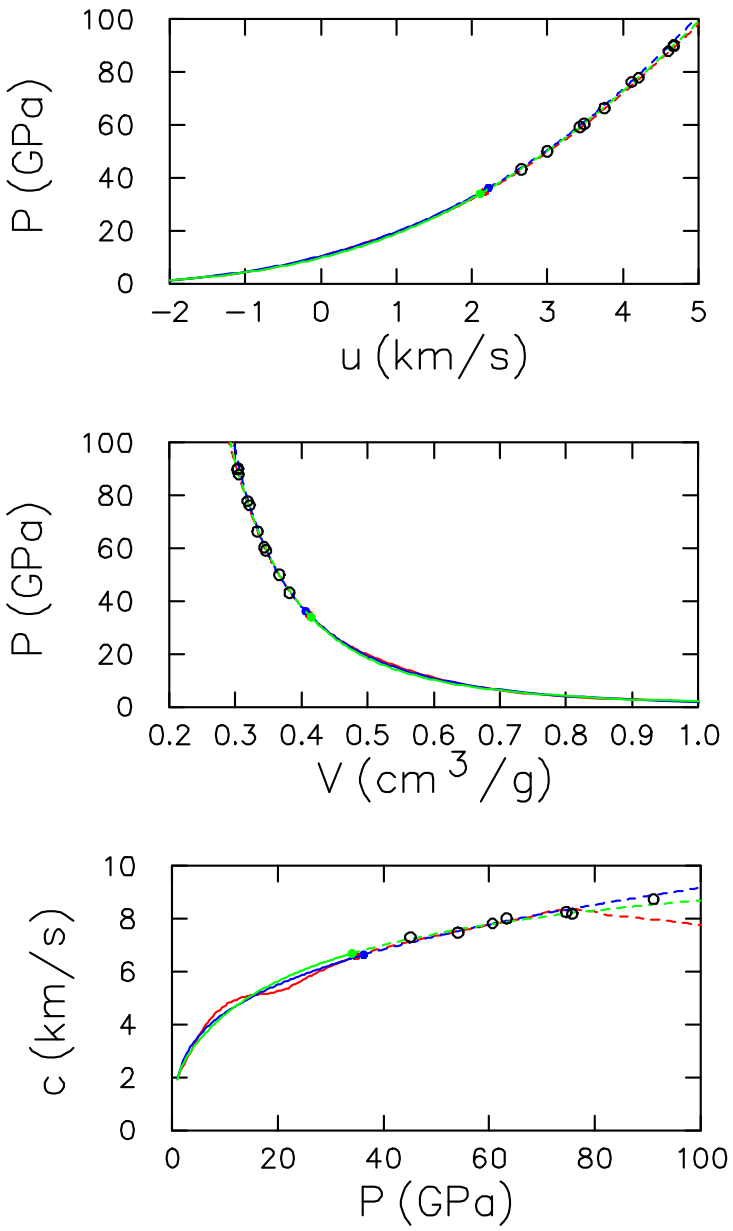

Figure 2: PBX 9501 product loci: red, blue and green curves correspond to models I, II, III, respectively. Solid curves are release isentrope from CJ state and dashed curves are detonation locus. Solid circles are CJ state of the models. Open circles are overdriven detonation wave data points from Fritz et al. [1996, tables I and III].

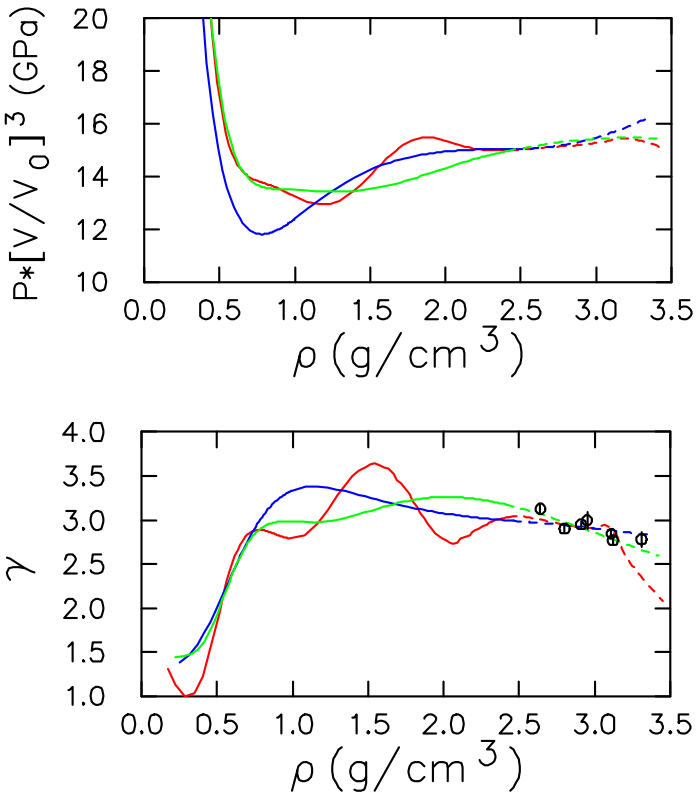

Figure 3: Plots of $P(V/V_0)^3$ and adiabatic index ($\gamma = \rho\, c^2/P$) versus density along PBX 9501 product loci: red, blue and green curves correspond to models I, II, III, respectively. Solid curves are release isentrope from CJ state and dashed curves are detonation locus. Open circles are overdriven detonation wave data points from Fritz et al. [1996, table III]. Lowest density corresponds to pressure of 0.1 GPa, and highest density to pressure of 100 GPa.

means of extrapolation. However, in contrast to interpolation, large errors can occur for extrapolations. As an example of this, the low pressure fit does poorly for the overdriven wave data. Similarly, the low pressure fit to the reactants Hugoniot of model III does not have the experimentally observed concavity in the (u_p, u_s)–plane for stronger shocks as seen in fig. 1. Second, extending the domain of a fit can lower the accuracy on the original domain. The difference between the two fits below the CJ pressure is evidence of this. We note that a fitting form can also be modified by adding degrees of freedom

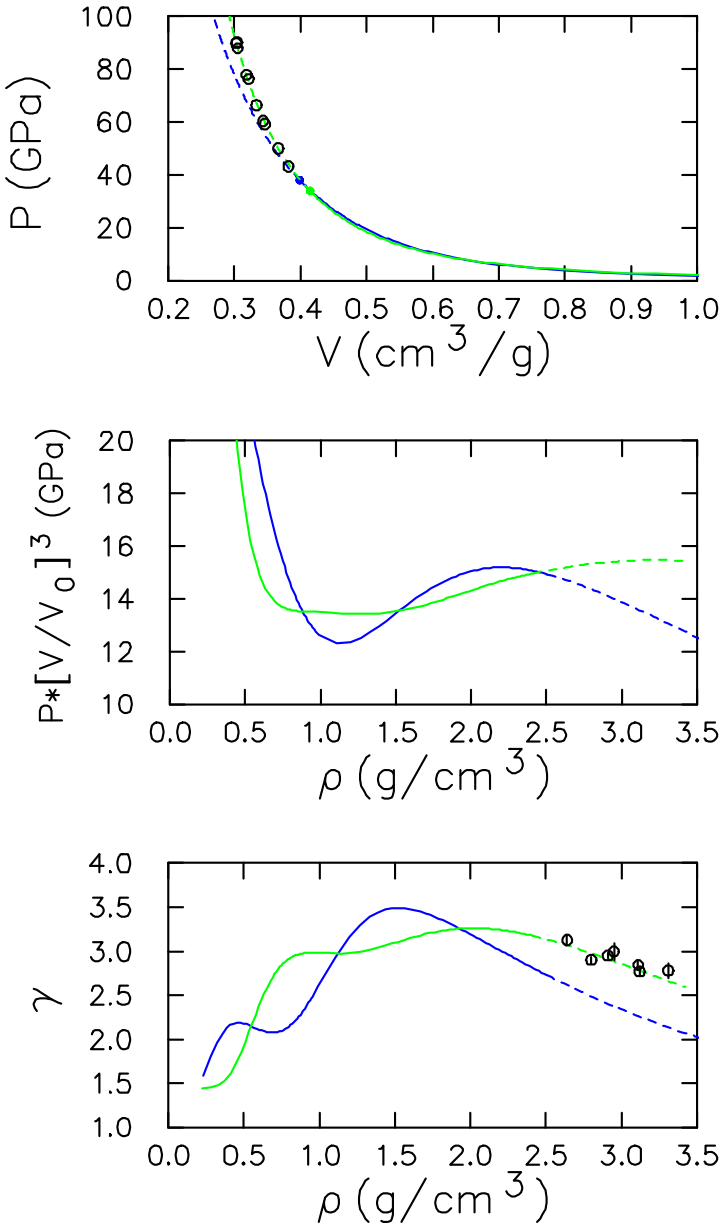

Figure 4: Comparison of JWL EOS fits for LX 14 products. Green curve uses parameters from model III [Tarver et al., 1996, table 2] and blue curve uses parameters from [Souers and Haselman, 1994, table 5-3].

to extend its domain of applicability; see for example, [Tang et al., 1998].

This illustrates a generic problem with empirical fitting forms that do not have a theoretical basis; extrapolation is error prone. Since domains are not usually specified, and for lack anything better, numerical simulations frequently use model equations of state outside the domain on which they have been calibrated. With the emphasis of a simulation code on robustness, users are typically unaware of errors that arise from extrapolating model equations of state.

3.3 Reactants and products Hugoniot loci

Key properties of a detonation wave can be inferred by combining the reactants Hugoniot locus and the products detonation locus. For the three models, these loci projected in the (u, P)–plane are shown in fig. 5. The importance of this plane stems from its use in the graphical construction of the solution to an impedance match problem.

Points on a steady reaction zone profile lie on the Rayleigh line; slope $\rho_0 D$, where D is the detonation wave speed. The Rayleigh line for the CJ detonation wave is also shown in the figure. The intersections of the loci with the Rayleigh line correspond to the CJ state (products locus) and the von Neumann spike (reactants locus). These states for the three models are given in the table 1.

The initial density of a PBX can vary depending on the pressing technique used to combine the grains with the binder. A higher density corresponds to decreasing the porosity. We note that the initial density assumed by the models differ by about 0.5 %.

The CJ temperature for model III is unreasonably high. This is in part due to the way in which temperature is constructed for an incomplete JWL EOS. Typically, the specific heat is assumed constant. Even with a constant specific heat, one has the freedom to pick a reference temperature at an arbirtray point. For temperature T_r at (V_r, P_r), a complete JWL EOS can be written as

$$P(V,T) = A\exp(-R_1 V/V_0) + B\exp(-R_2 V/V_0) + \frac{\omega}{V} C_v T \\ + \left(\frac{V_r}{V}\right)^{\omega+1} \left[P_r - \frac{A}{R_1}\exp(-R_1 V_r/V_0) - \frac{B}{R_2}\exp(-R_2 V_r/V_0) - \frac{\omega}{V_r} C_v T_r \right] .$$

Typically, T_r is implicitly chosen such that the last term vanishes. The JWL

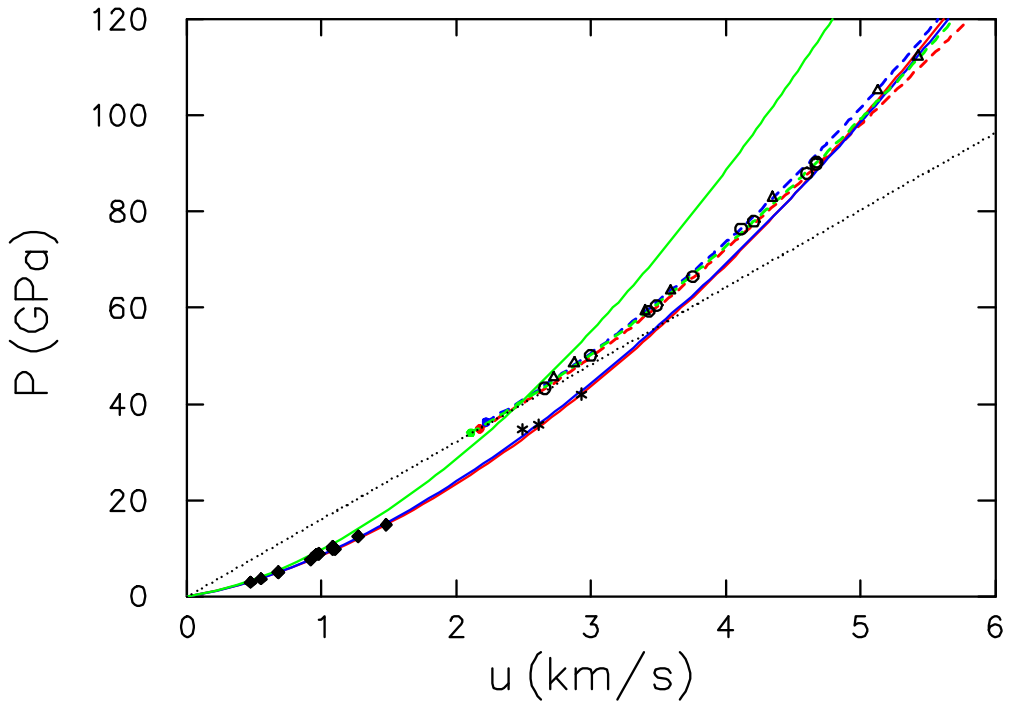

Figure 5: Detonation loci for PBX 9501: red, blue and green curves correspond to models I, II, III, respectively. Solid curves are unreacted ($\lambda = 0$) and dashed curves are fully reacted ($\lambda = 1$). Dotted black line is Rayleigh line through CJ state for model III. Solid circles are CJ state of the models. Open circles are overdriven detonation wave data points from Fritz et al. [1996, table I]. Open triangles are overdriven detonation data for PBX 9404 from Green et al. [1985, table II]. Solid diamonds are reactant Hugoniot data from Sheffield et al. [2004] and stars are from high pressure single crystal HMX experiments by Craig [Marsh, 1980, p. 595].

EOS then has the simple form,

$$P(V,T) = A\exp(-R_1 V/V_0) + B\exp(-R_2 V/V_0) + \frac{\omega}{V} C_v T \ , \qquad (1)$$

which reduces to an ideal gas EOS in the limit that V becomes large.

Furthermore, the specific heat C_v is typically chosen appropriate for low density gaseous products. However, the CJ state is above the normal density of the solid reactants. In this regime, the specific heat is comparable to that of a solid. A solid has a considerably higher specific heat than a typical

Table 1: Von Neumann spike and CJ states for detonation wave in PBX 9501 based on the model equations of state.

	Model I	Model II	Model III	
ρ_0	1.833	1.844	1.835	g/cm^3
D	8.77	8.86	8.80	km/s
VN spike				
P	56.9	59.0	39.6	GPa
ρ	3.07	3.11	2.54	g/cm^3
u	3.55	3.61	2.45	km/s
T	2581.	1801.	1550.	K
CJ state				
P	34.9	36.3	34.0	GPa
ρ	2.43	2.46	2.41	g/cm^3
u	2.17	2.22	2.11	km/s
T	3000.	3500.	5372.	K

gas since its vibrational degrees of freedom soak up more energy than the translational and rotational degrees of freedom of a gas. Thus, it would make more sense to use the CJ temperature as a reference to complete the JWL EOS. Unforturnately, there is no temperature data on the products in the vicinity of the CJ state. Hence there is large uncertainty in CJ temperature.

For model III, in contrast to the other models, the von Neumann spike pressure is only slighly larger than the CJ pressure. This is not consistent with VISAR measurements on the reaction zone profile of a steady detonation wave; see [Menikoff, 2006, Gustavsen et al., 1998a,b]. In addition, as seen in fig. 5, the Hugoniot locus of the reactants crosses the detonation products locus at a pressure only slightly higher than that of the von Neumann spike. This is not plausible. Both the low von Neumann spike pressure and the low crossing pressure of the loci are a consequence of the overly stiff reactants EOS.

For model I the loci cross at a pressure of about 90 GPa. It is possible at sufficiently high pressure that an HMX crystal becomes unstable and would decompose, or the reactant EOS may be softer at higher pressures than the

model indicates. Model II has been calibrated such that the loci do not cross. However, it should be noted that at high pressures the models amount to extrapolations based on empirical fitting forms. As pointed out previously, extrapolations suffer from the potential for large errors. Consequently, a model prediction on whether or not the loci cross at high pressure is very uncertain. The crossing of the loci would be of theoretical interest, even though present high explosive applications do not operate within this very high pressure regime.

3.4 ZND wave profile

With the addition of a reaction model, the steady CJ reaction zone profile is determined. It can be obtained by integrating the pair of ODEs

$$\begin{aligned} \frac{\mathsf{d}}{\mathsf{d}\xi}u &= \frac{V}{c_f^2-(D-u)^2}\left(\frac{\partial P}{\partial \lambda}\right)_{V,e}\mathcal{R}(V,e,\lambda)\ , \\ \frac{\mathsf{d}}{\mathsf{d}\xi}\lambda &= -\frac{\mathcal{R}(V,e,\lambda)}{D-u}\ , \end{aligned} \tag{2}$$

where c_f is the frozen sound speed determined by the partially burnt EOS, $(\rho c_f)^2 = -(\partial P/\partial V)_{s,\lambda}$, and $\mathcal{R}$ is the reaction rate. To complete the system, V and P are determined from the Rayleigh line, and e from Bernoulli's relation;

$$\begin{aligned} \Delta V &= -\Delta u/m\ , \\ \Delta P &= m\Delta u\ , \\ \Delta\Big[e+PV+\tfrac{1}{2}(D-u)^2\Big] &= 0\ , \end{aligned}$$

where $m = \rho_0 D$ is the mass flux through the front. The starting point for the integration is the von Neumann spike state. The particle velocity profiles for the three models are shown in fig. 6.

Model I uses an Arrhenius reaction rate. The reaction profile is compatible with VISAR data for a planar underdriven detonation wave; see [Menikoff, 2006, Gustavsen et al., 1998a,b]. Model II uses a P^n reaction rate, with reaction order slightly less than 1, that is calibrated to Pop plot data. It is in reasonable agreement with the curvature effect; see [Lambert et al., 2006]. The profiles for models I and II are comparable. The reaction zone width is less than the average grain size in PBX 9501; about 0.1 mm.

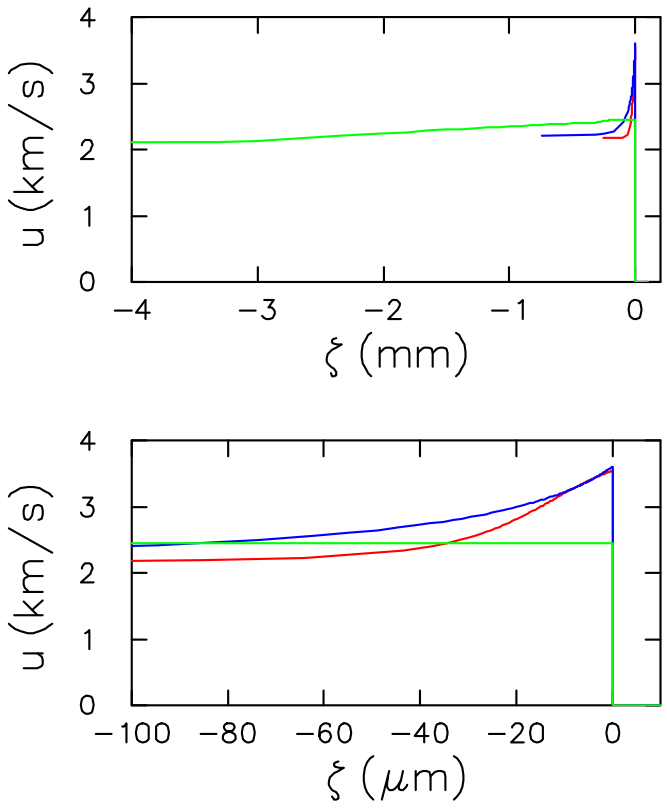

Figure 6: Steady state CJ reaction profile for PBX 9501: red, blue and green curves correspond to models I, II, III, respectively. $\zeta = x - Dt$ is spatial coordinate with origin at wave front. Bottom plot displays expanded spatial scale.

Model III uses an ignition and growth rate, which is the sum of terms proportional to P^n with different reaction orders to mimic subgrid surface to volume effects. It is calibrated to sideways plate push data; transverse expansion of rate stick confined by thin metal wall. The large reaction width for this model is inconsistent with resolved measurements of the reaction zone [Gustavsen et al., 1998a,b]. It appears that the rate parameters were used to compensate for the low von Neumann spike pressure from the overly stiff reactant EOS. A model with such a large reaction width would not be able to reproduce quantitatively the curvature effect since the local detonation velocity depends on the ratio of the reaction zone width to the radius of curvature of the front. This illustrates the need to validate a burn model by

comparing with experiments designed to measure several different aspects of detonation wave phenomena.

The ODEs for the reaction zone profile, Eq. (2), can be modified to allow for front curvature. These can be used to obtain the curvature effect or the $D(\kappa)$ relation needed for detonation shock dynamics. The detonation speed is the solution to an eigenvalue problem; given κ determine D such that the solution trajectory to the ODEs starting at state behind reactant shock passes through the critical point at which the flow is sonic and the reaction rate is balanced by geometric source term from the curvature.

The spatial location of the critical point is sensitive to the reaction order. With a first order reaction, as used in model I, the profile for planar wave ($\kappa = 0$) has an exponential tail, and the sonic point is at infinity. The ODEs represent a quasi-steady approximation that neglects transverse flow. This requires that the front curvature varies slowly over a length scale on the order of the reaction zone width. The approximation breaks down for a first order reaction. For model II the reaction order is chosen to be less than 1 in order that the reaction zone width is finite and the quasi-steady approximation can be applied.

For the pressure-dependent rate models, we note that the reaction zone profile is relatively insensitive to the assumption of pressure-temperature equilibrium; see for example, [Stewart et al., 2002]. However, for chemical rates the temperature is very important. In particular, the magnitude of the temperature variation within the reaction zone affects the stability of a propagating detonation wave; see [Menikoff, 2006].

3.5 Reactants expansion isentrope

There is a generic defficiency in the reactant EOS for all three models that is important for a relevant class of applications. Consider a detonation wave in a PBX reaching a boundary with air. The impedance mismatch results in a shock in the air and a strong reflected rarefaction in the PBX which quenches the reaction. The lead shock of the detonation wave imparts a high specific energy to the PBX. As the pressure in the rarefaction decreases, pressure-temperature equilibrium of the partially burnt PBX causes the density of the reactants to decrease below its ambient density.

Solid equations of state are designed for compression. Frequently, they become thermodynamically inconsistent in expansion. Pressure-temperature

equilibrium is equivalent to maximizing the mixture entropy,

$$S(V, e) = \lambda_1 S_1(V_1, e_1) + \lambda_2 S_2(V_2, e_2) \ ,$$

subject to the constraints

$$V = \lambda_1 V_1 + \lambda_2 V_2 \ ,$$
$$e = \lambda_1 e_1 + \lambda_2 e_2 \ .$$

The entropy of a thermodynamic consistent EOS is jointly concave in V and e. When both components are thermodynamically consistent, the mixture entropy is concave and has a unique maximum. Conversely, an equilibrium solution may not exist if V and e vary such that a component state crosses into a thermodynamically inconsistent region. This in fact occurs when expansion causes the density of the reactant to drop too low.

As an example, which can be readily analyzed, we consider the JWL EOS, Eq. (1). The square of the isothermal sound speed is

$$c_T^2(V, T) = \frac{V}{V_0}\left[A\, R_1 \exp(-R_1 V/V_0) + B\, R_2 \exp(-R_2 V/V_0)\right] \ .$$

When used for the reactants, $A > 0$ but $B < 0$. Moreover, $R_1 > R_2$. Consequently, $c_T^2 < 0$ and the EOS is thermodynamically inconsistent for

$$\frac{\ln\left[-(A\, R_1)/(B\, R_2)\right]}{R_1 - R_2} < \frac{V}{V_0} \ .$$

Substituting the values of the parameters for LX-14 reactants from [Tarver et al., 1996], one finds that $c_T^2 < 0$ for expansion greater than of 12.6 %. For the criticial compression, at which $c_T = 0$, the pressure is given by $P(T) = -1.09\,\mathrm{GPa} + 0.00219\,(\mathrm{GPa/K})\,T$. Partial burning can drive up the temperature. As an example, at half the model CJ temperature, the mimimum pressure is 5.8 GPa.

Numerical simulations frequently run into difficulties with P-T equilibrium of partially burnt explosives, especially at boundaries or interfaces, because of limitations on the domain of the EOS for the reactants model. If the PBX is mostly burnt the typical "fix" is to consider the PBX all burnt. An alternative workaround, in which the EOS is modified to extend its domain, will be discussed elsewhere. Modifying the EOS in a thermodynamically consistent manner has the advantage that the accuracy of the numerics can be checked by decreasing the cell size, *i.e.*, one can distinguish between numerical issues (verification) and modeling issues (validation).

4 Conclusions

The PBX 9501 models studied here illustrate several generic difficulties in developing and validating constitutive models for heterogeneous explosives:
1. For the phase space regime of interest there is no well established theory. Consequently, models are based on empirical fitting forms.
2. The data available to calibrate a fitting form are limited. For example, there is no temperature data on the reactants Hugoniot locus or for the products near the CJ state. The data for the reactants Hugoniot locus does not even extend up to the CJ pressure. Consequently, fitting forms are used to extrapolate data. Extrapolations have the potential for large errors. Molecular dynamics (MD) simulations are a promising approach for obtaining material property data in regimes (such as at high pressure and high temperature) that are either too difficult or too expensive to probe experimentally. To date MD results have been semi-quantitative; see for example, [Sewell et al., 2003].
3. Due to uncertainties in data, "good agreement" with a single experiment can be the result of compensating errors; such as adjusting rate parameters for defficiencies in EOS model. Thus it is important to test a model against more than one experiment. Data from different experiments are also needed to construct a model over an extended domain; such as overdriven detonation wave experiments for high pressure and cylinder tests for lower pressures. An important issue when comparing a model with multiple data sets is understanding experimental errors, both random and systematic.
4. Important data on the products EOS comes from integral experiments; such as release wave from overdriven detonation and cylinder tests. Testing constitutive model requires comparing measured profile data with hydro simulations using the model. A barrier to such comparisons is due to the lack of availability of data in electronic form. Though not discussed here, electronic form of gauge data from ignition experiments, such as [Gustavsen et al., 2002], would be helpful for the development of rate models.

Given the uncertainties from the factors listed above, there is a lot of variability in constitutive models that are compatible with available data. This is a critical issue since more and more research relies on simulations for which constitutive models are input. To assess the sensitivity of a simulation to uncertainties in material properties, it would be very useful to compare different constitutive models. The research community needs a program to facilitate such comparisons. Otherwise, despite the large amount of continu-

ing work, real progess will be very slow.

Nowadays every researcher has a dedicated PC with access to the internet. To take advantage of these technological advances, the research community needs to setup and develop a WEB based database for explosives. The database should include experimental data in electronic form and model parameters for various materials. By collecting the relevant data in one place, a researcher could more easily judge the merits of a particular model. Moreover, when material parameters are adjusted to obtain agreement with a new experiment, the needed data would be readily available to check for side effects modifying a model has on other phenomena previously fit. This would avoid the present tendency to view model validation as a one-off license for future use.

Comparing models would also be useful for establishing a models' domain of validity. This is an important issue for two reasons. First, with the advent of more and more powerful computers, simulations are possible on finer scales. This can be used, for example, in meso-scale simulations of hot-spot ignition to better understand the underlying physics and extend the predictive capabilities of burn models. It should be noted that finer scales require more accurate models. As discussed in subsection on the ZND wave profile, effective pressure dependent burn models are insensitive to the temperature. However hot-spot simulations require temperature sensitive chemical reaction rates. Consequently, equations of state used to model reactants and products with effective burn rates may not be applicable for meso-scale simulations.

Second, effective burn rates are generally calibrated to simple 1-D experiments. The fits tacitly assume the hot-spot distribution in the calibration experiments. These models do well for experiments with a similar hot-spot distribution. They are not accurate for other experiments, such as corner turning and the associated dead zone that develop. This is because the transverse flow gives rise to rarefactions that change the hot-spot distribution. Without a clear understanding of when a model is applicable, simulations can be misleading and result in incorrect conclusions or a poor design for an application.

Acknowledgements

This work was carried out under the auspices of the U. S. Dept. of Energy at LANL under contract W-7405-ENG-36. The author thanks Sam Shaw for enlightening discussion on equations of state and for providing the Sesame table he generated for PBX 9501 products.

References

W. C. Davis. Equation of state for detonation products. In *Eleventh (International) Symposium on Detonation*, pages 303–308, 1998.

W. C. Davis. Complete equation of state for unreacted solid explosive. *Combustion and Flame*, 120:399–403, 2000.

J. N. Fritz, R. S. Hixson, M. S. Shaw, C. E. Morris, and R. G. McQueen. Overdriven-detonation and sound-speed measurements in PBX 9501 and the thermodynamic Chapman-Jouguet pressure. *J. Appl. Phys.*, 80:6129–6149, 1996.

T. R. Gibbs and A. Popolato, editors. *LASL Explosive Property Data*. Univ. of Calif. Press, 1980.

W. A. Goddard, D. I. Meiron, M. Ortiz, J. E. Shepherd, and J. Pool. Annual technical report. Technical Report 032, Center for Simulation of Dynamic Response in Materials, Calif. Inst. of Tech., 1998. `http://www.cacr.caltech.edu/ASAP/publications/cit-asci-tr/cit-asci-tr032.pdf`.

L. Green, E. Lee, A. Mitchell, and C. Tarver. The supra-compression of LX-07, LX-17, PBX-9404, and RX-26-AF and the equation of state of the detonation products. In *Eighth (International) Symposium on Detonation*, pages 587–595, 1985.

R. L. Gustavsen, S. A. Sheffield, and R. R. Alcon. Detonation wave profiles in HMX based explosives. In *Shock Compression of Condensed Matter – 1997*, pages 739–742, 1998a.

R. L. Gustavsen, S. A. Sheffield, and R. R. Alcon. Progress in measuring detonation wave profiles in PBX 9501. In *Eleventh (International) Symposium on Detonation*, 1998b.

R. L. Gustavsen, S. A. Sheffield, R. R. Alcon, and L. G. Hill. Shock initiation of new and aged PBX 9501. In *Twelve (International) Symposium on Detonation*, 2002.

B. F. Henson, B. W. Asay, L. B. Smilowitz, and P. M. Dickson. Ignition chemistry in HMX from thermal explosion to detonation. In *Shock Compression of Condensed Matter – 2001*, pages 1069–1072, 2002.

L. G. Hill. Development of the LANL sandwich test. In *Shock Compression of Condensed Matter – 2001*, pages 149–152, 2002.

R. S. Hixson, M. S. Shaw, J. N. Fritz, J. N. Vorthman, and W. W. Anderson. Release isentropes of overdriven plastic-bonded explosive PBX 9501. *J. Appl. Phys.*, 88:6287–6293, 2000.

J. W. Kury, H. C. Honig, E. L. Lee, J. L. McDonnel, D. L. Ornellas, M. Finger, F. M. Strange, and M. L. Wilkins. Metal acceleration by chemical explosives. In *Fourth (International) Symposium on Detonation*, pages 3–13, 1965.

D. E. Lambert, D. S. Stewart, S. Yoo, and B. L. Wescott. Experimental validation of detonation shock dynamics in condensed explosives. *J. Fluid Mech.*, 546:227–253, 2006.

S. P. Marsh, editor. *LASL Shock Hugoniot Data*. Univ. of Calif. Press, 1980.

R. Menikoff. Detonation waves in PBX 9501. *Combustion Theory and Modelling*, (submitted), 2006. LA-UR-06-0166, `http://t14web.lanl.gov/Staff/rsm/Preprints/DetWave.pdf`.

R. Menikoff and T. D. Sewell. Complete equation of state for beta-HMX and implications for initiation. In *Shock Compression of Condensed Matter – 2003*, pages 157–160, 2004.

T. D. Sewell, R. Menikoff, D. Bedrov, and G. D. Smith. A molecular dynamics simulation study of elastic properties of HMX. *J. Chem. Phys.*, 119:7417–7426, 2003.

M. S. Shaw, 2004. private communication.

S. A. Sheffield, R. L. Gustavsen, R. R. Alcon, D. L. Robbins, and D. B. Stahl. High pressure Hugoniot and reaction rate measurements in PBX 9501. In *Shock Compression of Condensed Matter – 2003*, pages 1033–1036, 2004.

P. C. Souers and L. C. Haselman. Detonation equations of state at LLNL. Technical Report UCRL-ID-116113, Lawrence Livermore National Laboratory, 1994. `http://www.llnl.gov/tid/lof/documents/pdf/224523.pdf`.

D. S. Stewart, S. Yoo, and W. C. Davis. Equation of state for modeling the detonation reaction zone. In *Twelve (International) Symposium on Detonation*, pages 624–631, 2002.

P. K. Tang, R. S. Hixson, and J. N. Fritz. Modeling PBX 9501 overdriven release experiments. In *Shock Compression of Condensed Matter – 1997*, pages 365–368, 1998.

C. M. Tarver, W. C. Tao, and C. G. Lee. Sideways plate push test for detonating solid explosives. *Propellants, Explosives, Pyrotechnics*, 21:238–246, 1996.